Asadzadeh, S., de Souza Filho, C. R. (2024):
REMOTE SENSING ANALYSIS AND NUMERICAL MODELLING OF SURFACE TEMPERATURE ANOMALIES OVER PETROLEUM ACCUMULATIONS: A CASE STUDY OF THE ALBORZ OILFIELD, CENTRAL IRAN. - Journal of Petroleum Geology, 47, 2, 215-230.

https://doi.org/10.1111/jpg.12857

Remote sensing analysis and numerical modeling of surface temperature anomalies over petroleum accumulations: A case study of the Alborz oilfield, Central Iran

Saeid Asadzadeh[†*]
Carlos Roberto de Souza Filho

University of Campinas (UNICAMP); Rua Carlos Gomes, 250, 13083-855 Campinas, SP, Brazil
[†] Current address: Section of Remote Sensing and Geoinformatics, Helmholtz Center Potsdam, GFZ German Research Center for Geoscience, 14473 Potsdam, Germany
[*] Corresponding author, saeid@gfz-potsdam.de

Abstract

Petroleum accumulations have been known to coincide with either positive or negative temperature anomalies. Such anomalies are conventionally detected using in-situ temperature measurements made at shallow holes of 1–3m deep. The data provided in this way, however, are sparse and costly and require intensive fieldwork and collection time. This article explores the possibility of detecting thermal anomalies associated with petroleum entrapment using satellite-derived land surface temperature data. For this aim, a robust correction scheme based on a physically-based land surface model is applied to nighttime kinetic temperature data derived from NASA's ASTER instrument. The numerical model, known as SKinTES, attempts to simulate the diurnal effects and remove them from the measured temperature data to yield a residual temperature anomaly map. The performance of this methodology was tested over the Alborz oilfield located on an anticline of the same name in the Qom region of Central Iran. The area has an arid to semi-arid climate and the surface geology is dominated by outcrops of the Lower Miocene Upper-Red Formation. The modeling approach successfully highlighted several negative temperature anomalies over the oil-bearing parts of the Alborz structure. In comparison to the uncorrected data, the anomalies were shown to be highly enhanced in both spatial and magnitude terms. In addition, time series analysis indicated that the temperature anomalies are consistent over time. The authenticity of the anomalies was confirmed by a suite of in-situ temperature measurements made at shallow holes. In the end, a unifying framework was proposed to explain the occurrence of both the negative and positive temperature anomalies over petroleum accumulations. The new modeling and correction scheme is expected to broaden the application of remote sensing land surface temperature data not only in petroleum exploration but also in other types of geothermic investigations, including geothermal exploration.

Keywords: land surface temperature; residual temperature anomaly map; subsurface geothermic; exploration; Qom region.

1. Introduction

Petroleum accumulations have been known to coincide with temperature anomalies since the early days of exploration (Meyer and McGee, 1985; Roberts, 1981) and the near-surface temperature measurements have been widely used in petroleum-related studies (Eppelbaum et al., 2014). The nature and cause of such temperature anomalies, however, remain controversial. While some studies have emphasized the occurrence of positive thermal anomalies above hydrocarbon-bearing reservoirs ("hot anticlines"), others have recorded the presence of negative temperature anomalies (Blackwell, 1986; Fons, 1999; Merriam, 2004; Zielinski and Bruchhausen, 1983) (Fig. 1). Negative temperature anomalies are believed to arise from the insulation effects of petroleum accumulation against the upward, conductive flow of heat from the basin basement to the Earth's surface (Chakraborty et al., 2010; Fons, 2000; Fons, 2001). The magnitude of a negative temperature anomaly measured at the surface can vary from ∼1 to 8°C following the corrections for humidity, thermal inertia, and altitude (Fons, 2001). Within boreholes, temperature anomalies can reach up to 10°C relative to the temperature calculated from the geothermal gradient of the area, which when projected to the Earth's surface can reach the order of ∼1°C. However, measured anomalies of up to 8°C, particularly over the productive portions of some oilfields, have also been reported (Fons, 2000). Such observations have further been substantiated by numerical modeling. By projecting the difference between observed and modeled geothermal gradients to the surface, a negative temperature anomaly in the order of 5–7°C was predicted to occur above the oilfields of the Cambay Basin in India (Chakraborty et al., 2010).

The magnitude of a temperature anomaly is speculated to be controlled by the thickness and depth of the associated oil pool: the greater the thickness, the higher the anomaly; albeit it is inversely related to the depth of the accumulation. The intensity of the anomaly is therefore thought to be directly linked to the petroleum contents of a trap, with pay zones of moderate thickness being the most difficult to detect using the temperature profiling method. Statistically, negative anomalies are reported to occur above >75% of oil and gas accumulations (Fons, 1999; Fons, 2001; Fons and Donovan, 2000).

On the other hand, the magnitude of positive geothermal anomalies overlying petroleum accumulations is reported to vary from 0.3 to 2.0°C at the measurement depths of 3 to 30 m (McGee et al., 1989); although values in the order of 0.5–1.0°C have been recorded very close to the surface (i.e. at 1.2 m depth) (Zielinski and Bruchhausen, 1983). At deeper boreholes drilled onto oil-bearing structures, however, anomalous temperatures as high as 5.6–8.3°C have been detected (Merriam, 2004). The temperature anomalies, which tend to occur over at least 70% of the studied cases (McGee et al., 1989; Merriam, 2004; Meyer and McGee, 1985) are generally apical[1] in shape and coincide with the outline of the underlying accumulations. "Halo" type anomalies[2] are less often detected at the edges of petroleum reservoirs (Fons, 1984). The transport of heat in this model is attributed to the vertically migrating warm water from the apex/crest of the structure to the near-surface environment (Roberts, 1981).

Several other studies have reported the occurrences of both positive and negative temperature anomalies in a petroleum province. For example, by extrapolating bottom-hole temperature data to the surface, Ibrahim (1994) demonstrated that hydrocarbon traps in the Southern North Sea area are associated with both low (negative) and high (positive) surface temperature anomalies. A similar pattern was also noted to occur in the Volga-Ural petroleum province (Parfenenko, 1979).

The methods routinely used to collect near-surface temperature data in petroliferous basins include in-situ temperature measurements made at shallow holes of about 1–3m deep

---

1- An apical anomaly typically emerges at the apex of a petroleum accumulation (in plain view) and is characterized by an area of high values surrounded by a lower background.
2- In a halo pattern, anomalous readings are aligned over the edges of the underlying accumulation.

(Blackwell, 1986; Fons, 2001; McGee et al., 1989; Zielinski and Bruchhausen, 1983). The shallow surveying intends to avoid disturbances caused by surface processes. The collected data, however, is sparse and costly and requires intensive fieldwork and collection time. In addition, owing to the complexity of surface temperature patterns in space and time (due to diurnal and seasonal effects), the sparse measurements obtained from this approach cannot practically provide values over wide areas, and in most cases, on-site (field) calibration is deemed essential to obtain comparable results. The complications associated with data collection and interpretation together with the controversy on the nature of geothermal anomalies themselves have contributed to the relatively limited use of temperature methods in hydrocarbon exploration (Blackwell, 1986).

Surface temperature data sets can alternatively be obtained using thermal infrared remote sensing data. Since remote sensing data are acquired simultaneously, environmental conditions (e.g. atmospheric conditions, diurnal/seasonal timing, etc.) are consistent within a given scene. Thus, by applying proper correction procedures, the data can provide uniform and seamless temperature readings over large regions (Li et al., 2013). With improvements in the spatial resolution (i.e. <100 m) and accuracy (i.e. $\pm 1°C$) of satellite-derived surface temperature data, it is now feasible to use such datasets to locate geothermal anomalies related to a number of geological processes including petroleum entrapment. An example of this approach is provided by the analysis of data from the Advanced Spaceborne Thermal Emission and Reflection Radiometer (ASTER) over the Cambay basin (India) in search of petroleum-related surface temperature anomalies (Gupta et al., 2009).

Daytime land surface temperature (LST) data, however, are in general overwhelmed by the warming effect of sunlight and the effect of topographic slope and aspect (see, for example, Fig. 2), making the use of such data sets difficult for geothermal mapping (Coolbaugh et al., 2007). During the night, the interfering effects of topography and solar irradiance are greatly reduced, and prospective subsurface thermal anomalies thus become more noticeable. For instance, Majumdar et al. (2010) indicated that ASTER nighttime data in the Cambay Basin were better able to detect low-temperature anomalies arising from petroleum accumulations. But even nighttime data are liable to be affected by extraneous factors such as surface compositional heterogeneity (i.e. thermal inertia, surface albedo, surface emissivity, and surface roughness length), soil moisture content, meteorological forcing, and the air temperature lapse rate induced by terrain elevation (Blackwell, 1986; Coolbaugh et al., 2007).

Successful mapping of petroleum-related temperature anomalies with magnitudes that are typically $\pm 5\%$ of the background requires that a robust correction scheme is applied to the remotely sensed temperature data. This can be achieved by coupling the satellite-derived surface temperature data with physically-based land surface models aimed to counteract the effects of surface processes and compensate for the limited penetration depth of thermal infrared data. A land surface model uses quantitative techniques to simulate the exchange of energy and water at the air-land boundary to predict diurnal temperature patterns. A recently developed model of this type is the Surface KINetic TEmperature Simulator (SKinTES) which was specifically designed to model temperature patterns over geologically and topographically complex terrain (Asadzadeh and Souza Filho, 2023).

With respect to this background, this article attempts to investigate the occurrences of temperature anomalies in a petroliferous area in the Qom region, Central Iran, focusing on the Alborz oilfield. The work aims are (i) to investigate the type, magnitude, extent, and persistence of surface temperature anomalies in the study area using ASTER-derived nighttime kinetic temperature data corroborated by *in-situ* temperature measurements, (ii) to apply advanced numerical methods offered by the SKinTES model to remove the effects of surface processes from remote sensing temperature data and to highlight/isolate the contribution of subsurface geothermic related to petroleum entrapment, (iii) to investigate the extent to which this temperature method could be used for the regional targeting of prospective areas, (iv) to infer possible mechanisms by which heat is transferred to the surface and to attempt to provide a unifying framework to explain both the positive and negative types of temperature anomalies observed in petroliferous basins.

The underlying assumption of this methodology is that the subsurface flow continues up to the surface and manifests as an increase or decrease in the skin surface temperature patterns at a level that is reliably detectable by a remote sensing system. Accordingly, when thoroughly modeled by a land surface model, the prospective anomaly can confidently be isolated from diurnal temperature variations, giving rise to a residual temperature map over a target area. Empirical evidence shows that this is a reasonable assumption and that temperature anomalies can indeed emerge onto the surface (Fons, 2001; Zielinski and Bruchhausen, 1983). Because no source or sink for heat is included in the model, depending on the type of geothermal anomalies, the simulated surface temperature values will be over-estimated (sink) or under-estimated (source) when compared to measured data contributing to either negative or positive anomalies in a residual temperature map.

2. Geologic framework of the study area

The study area lies within the Saveh-Qom basin in Central Iran (Fig. 3). The stratigraphy of the basin consists of the upper Eocene – lower Oligocene Lower-Red Formation (LRF), Oligo-Miocene Qom Formation, and upper Miocene Upper-Red Formation (URF). The LRF comprises marls, shales, siltstones, and sandstones conformably overlain by the marine succession of the Qom Formation (Fig. 3). A sequence of halite-dominated evaporites at the base of the LRF has partly intruded into the overlying strata in the form of salt diapirs, which include the Kuh-e-Namak salt dome to the west of the study area (Fig. 3). The approximately 1000-m-thick Qom Formation consists of limestones, marls, and bituminous shales, which is overlain by a thick sequence of clastic-dominated sediments of the URF. The URF is made up of interbedded reddish sandstones, marly siltstone, and conglomerate whose drilled thickness in this region is about 3000 m (Asadzadeh and Souza Filho, 2020a; Morley et al., 2009).

The porous and fractured limestones of the Qom Formation constitute the reservoir at Alborz field sealed above by evaporitic units at the base of the URF. Organic-rich shales and mudstones of the Qom Formation have been identified as potential source rocks (Abbasi et al., 2020). The structure at Alborz comprises a detachment fold extending for over 50 km in a NW-SE direction. The reservoir is charged with oil, underfilled, and severely overpressured. More than fourteen wells have been drilled into the structure of which at least four are dry holes (Fig. 3). The thickness of the pay zone is approximately 200 meters, and the oil accumulations occur at a depth of around 3 km beneath the surface (Morley et al., 2013). The outline of the reservoir is yet to be fully appraised by drilling. Previous studies in the area including geochemical and remote sensing microseepage characterization are reported in detail in Asadzadeh and Souza Filho (2020a) and Asadzadeh and Souza Filho (2020b).

The Alborz anticline is characterized by a low-relief topography and altitude that ranges from 830 m to 1200 m. The surface geology consists of well-exposed outcrops of the URF. The climate in this region is arid to semi-arid with annual precipitation of less than 150 mm/year, and large daily and annual temperature variations ranging from −10°C to 45°C. The sparse vegetation coverage renders this location ideal for remote sensing temperature mapping.

3. Methods and models

3.1. Remote sensing land surface temperature data

The ASTER Thermal Infrared (TIR) instrument on NASA’s Terra satellite collects day- and nighttime thermal data at wavelengths between 8–12 µm in five multispectral bands from which land surface temperature (and emissivity) is determined using the temperature-emissivity separation algorithm. The temperature product has a spatial resolution of 90m and constitutes one of the highest spatial resolution remote sensing datasets available for geologic studies at the present day.

The nighttime surface kinetic temperature data over the study area were derived from the AST08 standard product corrected by the MODIS Model for atmospheric moisture profile (*earthdata.nasa.gov*). Four cloud-free nighttime scenes collected during different seasons between 2015 and 2019 were selected from the set of existing scenes in the EarthExplorer archive. New thermal datasets were additionally acquired on the night of 15 August 2020. This together with a daytime temperature product acquired on 10 August 2020 was used for setting up the model (see below).

The stripping noise inherent to ASTER temperature data was removed by employing the Fast Fourier Transform (FFT). To do so, the noise component of each scene was detected and removed in the frequency domain and the outcomes were subsequently converted back to the image domain. To eliminate data misalignment, all datasets were carefully orthorectified using the RPC (rational polynomial coefficients) model of the sensor, in conjunction with a set of ground control points manually collected over each scene and a digital elevation model obtained from the ALOS World 3D dataset at 30m spatial resolution (JAXA, Japan). The de-noised datasets were converted to absolute temperature and then color-coded to facilitate the analysis of temperature trends and their spatial distribution patterns over the oilfield. Correction for seasonal temperature variation was deemed unnecessary because the patterns of each scene were compared in a relative manner to each other. Finally, to make sure that the potential anomalies were not contaminated by green vegetation, the normalized difference vegetation index (NDVI) was calculated over the study area and used to isolate the pixels associated with green vegetation (NDVI >0.2).

3.2. Numerical modeling of land surface temperature

A recently developed land surface model called SKinTES was used to simulate the surface temperature patterns over the study area, and the results were compared to the ASTER-derived surface kinetic temperature data from 15 August 2020. The underlying hypothesis of the model is that by modeling surface processes and removing their effects from measured temperature data, the subtle temperature anomalies relevant to subsurface geologic processes (here petroleum entrapment) are uncovered in the form of residual temperature anomalies of either positive or negative form. It was assumed that the subsurface heating component is only present in the remotely sensed surface temperature data. Given that the model lacks a source of subsurface heat, depending on the type of subsurface anomalies, the simulated data over-, or underestimates the temperature patterns when compared to measured data. In other words, the model removes the diurnal and terrain effects (i.e. topographic slope-aspect and altitude, surface albedo, thermal inertia, soil moisture contents, and meteorological forcing) from the measured data and serves to intensify the temperature anomalies. The structure of the model and the procedures used for model setup and parameter estimation are briefly described in appendices A and B.

3.2.1. Residual temperature mapping

To detect anomalies, surface temperature values are typically compared with readings from a nearby reference area away from petroleum accumulations, preferably with the same lithologic composition. This strategy can help to eliminate the effects of spatially variable thermal inertia arising from the presence of different rock units. The measured and modeled temperature data, on the other hand, are compared differently. In the statistical approach, the mean difference between the observed and the modeled data is minimized using variance minimization techniques (Malbéteau et al., 2017). Other techniques use the concept of reference bias (which is the difference between observed and modeled temperature data in a reference area) to contrast the two datasets (Romaguera et al., 2018). Here, the model-simulated temperature data was directly subtracted from the measured data to yield a residual temperature anomaly map.

3.3. In-situ temperature measurement

In-situ temperature measurements were conducted during daytime hours between March 12 and 17, 2019, aiming to validate the authenticity of the temperature anomalies derived from the ASTER data and the numerical modeling. The process involved *in-situ* surface (and near-surface) temperature measurements at sparse stations ($n = 40$) along profiles that crossed the petroleum-bearing zones of the area (Fig. 3). We used a digital thermometer (Hanna model CheckTemp; Fig. 4) with an accuracy better than ± 0.2°C over the range between -30 and 120°C and a resolution of 0.1°C. The temperature measurements were made at a depth of ∼1–5 mm (to represent the skin surface temperature) and within auger-made drill holes of ∼15–20 cm deep (to represent the subsurface temperature) (Fig 4). The temperatures were recorded once the thermometer was stabilized (stabilized temperature). Typically, the subsurface temperature is measured at greater depths to avoid the diurnal effects, but due to complications in logistics, the holes remained confined to ∼20 cm depth. In addition, temperature measurement concurrent with the satellite overpass was not logistically feasible nor was it possible to collect data at night.

During the course of this campaign, the weather was partly to mostly cloudy with no precipitation and very mild winds. The soil was relatively dry near the surface, although variation in the soil moisture content was considerable both between measurement sites and across the depth intervals. We attempted to measure temperature at multiple sites dozens of meters apart and then average the readings to represent a station. The resulting data was then compared and correlated with the corresponding pixels extracted from the LST data. Likewise, the measurement points lying within each image pixel were averaged before comparison.

4. Results

As noted above and depicted in Fig. 2, the daytime temperature data is adversely affected by solar heating and topographic effects. As a result, the surface temperature data recorded in the morning (i.e. at 10:30 a.m.) exhibits high magnitude and a wide range of variability, spanning between 308 and 343 K, marking a temperature difference (ΔT) >35°C. In this image, temperature values are notably high across a large part of the area, with the lowest values being recorded along the steep slopes in the SW. The city of Qom stands as a sizable, low-temperature anomaly at the bottom center of the image. The vegetated areas in the NE and south of the area also show comparably lower temperatures. On the other hand, the Alborz anticline (indicated by a blacked dashed line in Fig. 2) retains a relatively uniform trend of elevated temperature values.

The nighttime temperature data collected over four different dates are shown in Fig. 5. During the night, a large portion of the heat dissipates away from the surface, resulting in a noticeable reduction in both the absolute temperature values and their variability. In this context, the temperature range (ΔT) varies from a minimum of 5°C in Fig. 5c to a maximum of 11°C in Fig. 5d, with the datasets from other dates falling in between. Despite the substantial differences in the spatial pattern of the LST data between day- and nighttime, the general pattern observed in the nighttime datasets remains relatively consistent over time (Fig. 5). Here, paved roads appear warm (black arrows in Fig. 5a), and the vegetated areas (i.e. irrigated lands on either side of the anticlinal structure: marked by white arrows in Fig. 5a) maintain low-temperature values in all of the maps shown in Fig. 5; although the effect is reduced in Fig. 5b, which corresponds to a period of no irrigation in the autumn. The salt diapir in the west of the study area (S in Fig. 5b) is associated with higher temperatures relative to its surroundings (particularly in its northern margin). In contrast, the playa encircling the salt diapir (P in Fig. 5b) represents spatially variable patterns across the maps in Fig. 5. In these maps, the effect of air temperature lapse rate is visible as low-temperature values over the highlands to the SW of the area, and the highest rate is seen in Fig. 5c (marked by L).

By contrast, the temperature pattern over the URF outcrops appears to show little variations in relative terms, particularly over the extent of the Alborz anticline. As depicted in Fig. 5a, at least five low-temperature anomalies can be recognized over the structure, of which four are located on the eastern side of Alborz coinciding with the southern limb of the anticline. A broadly similar pattern is observable in the temperature maps from other dates (Figs. 5b-d), regardless of the absolute values. In other words, the anomalies appear to be consistent over the analyzed period. The temperature profile in Fig. 6 (corresponding to A–B in Fig. 5b) indicates that the outlined anomaly is, on average, 1.5°C cooler than the surrounding area.

The residual temperature anomaly map obtained by subtracting the model-simulated data from the measured LST data is presented in Fig. 7. The Root Mean Square Error (RMSE) and the Mean Bias Deviation (MBD) between these two datasets are equal to 3.5°C and 0.44°C, respectively. It is notable that the modeled data overestimated the temperature pattern over most parts of the petroleum reservoir, giving rise to a negative residual temperature anomaly when subtracted from the measured satellite data.

Based on Fig. 7, the residual temperature values range from -5 to $+6$°C, of which the negative temperature anomalies largely coincide with the outline of the Alborz oil reservoir. Although the map does not cover the entire study area, it confirms the authenticity of at least four anomalies recognized in Fig. 5a. However, in comparison, the extent of the anomalies appears to be broadened and the corresponding temperature profile (e.g. dashed line in Fig. 6) illustrates a highly enhanced thermal anomaly. The extent to which the negative temperature anomalies coincide with the outline of the underlying reservoir is not yet fully recognized, but remarkably, the most productive oil wells of the field, comprising the blown-out well 5-Alborz (see Asadzadeh and Souza Filho, 2020a for details) appears to have been drilled over, or in the vicinity of, a negative temperature anomaly. In contrast, several dry wells have been drilled in areas with insignificant temperature anomalies. The anomalous zones distinguished in Fig. 7 are also spatially closely correlated to areas in which petroleum microseepage systems have been previously detected (shown by dotted white lines in Fig. 7) using the spectral analysis of multispectral remote sensing data (Asadzadeh and Souza Filho, 2020a). Contrasting with the oil-bearing regions, the salt diapir in the west of the study area appears to be associated with a positive temperature anomaly (Fig. 7).

The in-situ temperature data collected at the surface and in the shallow drill-holes range from 7.7°C to 34.1°C and from 10.8°C to 18.4°C, respectively, with the latter showing a closer relationship with the residual temperature data (circles in Fig. 7). In this data suite, the lowest recorded values (dark blue to cyan) typically coincide with negative temperature anomalies and vice versa. The highest values (green to red) coincide with either the margins of the structural trap or the edges of negative temperature anomalies exhibited in Fig. 7. The same dataset maintains a strong correlation (R^2 = 0.65) with remotely sensed LST data including, for example, the dataset acquired on 10 October 2017 (Fig. 8). In comparison, however, it systematically under-estimates the remotely sensed temperature values, particularly towards the lower end of the range where the bias exceeds 4°C.

5. Discussion

Nighttime data, although more informative for surface temperature mapping than daytime data (Fig. 5), cannot be used straightforwardly to target the subsurface geothermic component arising from petroleum entrapment, because the magnitude of the anomalies is not significantly different from the background and because the anomalies are non-unique and ambiguous particularly when interpreted in isolation. This is because spatial variability in parameters like surface albedo, lithology, and soil moisture contents is likely to produce a similar pattern. In this context, the close correlation between the temperature anomalies (Fig. 7) and the microseepage-affected zones identified in previous studies (Asadzadeh and Souza Filho, 2020a) on the one hand corroborates the results obtained from surface temperature mapping; but on the other hand, it may reflect the difficulties associated with the temperature method when applied to petroliferous regions.

A microseepage-affected area is typically characterized by iron bleaching and the formation of secondary minerals comprising clays (Asadzadeh and Souza Filho, 2017). The consequence of this is changes in the physicochemical properties of the sedimentary strata including an increase in the albedo of the surface (induced by bleaching) and a decrease (increase) in the bulk thermal (hydraulic) properties of the near-surface constituents induced by the presence of excessive clays (Abu-Hamdeh and Reeder, 2000). The cumulative results of this suite of changes are the low-intensity temperature anomalies observed in the microseepage-affected zones, as is evident in this particular area (e.g. Fig. 5).

Without the use of numerical modeling to comprehensively account for the interference effects of diurnal temperature variations relevant to surface albedo, emissivity, surface thermal properties, soil porosity, soil moisture contents, and topographic factors, one cannot confidently attribute the low-temperature anomalies to subsurface processes, as is the case with Fig. 5. Once the effects of the noted parameters are modeled and removed by applying the physically-based numerical model, the resulting map can not only highlight the contribution of the subsurface thermal regime associated with petroleum accumulations but also can result in enhanced temperature anomalies both in spatial and absolute terms (Fig. 7).

Here, direct subtraction of measured and simulated temperature data was possible thanks to the comprehensive modeling approach which took into account the effects of all the relevant variables. By direct subtraction, however, all the uncertainties are accumulated in (i.e. transferred to) the residual temperature data. These include uncertainties in the numerical model and/or the input parameters, uncertainties in the retrieval of LST data from thermal infrared images, and instrumental noise. For instance, the uncertainty associated with the stripping noise in the day- and nighttime temperature data was estimated to be at least +0.1°C and +0.4°C, respectively. The uncertainty of the model output (i.e. the detection limit) was estimated to be in the order of 2–3°C (Asadzadeh and Souza Filho, 2023), which is less than the magnitude of the negative temperature anomalies (i.e. -5°C) shown in Fig. 7. This means that the obtained results are still valid at this level of uncertainty. The magnitude of the yielded anomalies is also in good agreement with the negative temperature anomaly (i.e. 5–7°C) predicted by Chakraborty et al. (2010) in the Cambay Basin using numerical modeling. Note that the detection limit of other similar methodologies varies from 2°C to 5°C (Gutiérrez et al., 2012; Romaguera et al., 2018).

In contrast, the positive temperature anomaly observed over the salt dome (Fig. 7) is likely due to the high conductivity of salt (the salt diapir is composed of 90% salt) and the transport of anomalous heat to the surface by active diapirism in this area. The low-temperature anomaly over the surrounding playa, however, is likely due to the combined effect of the high albedo of the playa and the rapid cooling rates of salty soils during the night. Because of the rapid dissolution and precipitation of salt on the surface following a precipitation event, the albedo of the surface appears to be highly dynamic over time and so are the surface temperature patterns recorded above it (see Fig. 5). Such results suggest that if the presence of salt in the soil is not identified and modeled accordingly, it could constitute a source of false-positive anomalies in desert environments. Variability in the thickness and properties of the soil cover can also have a negative effect on the model-simulated results because the SKinTES model assumes a uniform and homogeneous soil profile during the modeling process. Typically, a thin soil layer overlying impermeable bedrocks can contribute to lowering the level of thermal inertia and thus the diurnal temperature fluctuations recorded by the sensing system (Nasipuri et al., 2006).

Another source of false-positive anomalies when applying the temperature technique to petroliferous basins is revealed to be shallow groundwater flow. The groundwater flow regime can interfere with the surface temperature measurements in two ways: (i) water tables within the range of annual temperature variation (i.e. depth of 5–15m) can constitute a positive anomaly (heat source) in the winter and a negative anomaly (heat sink) in the summer (see Becker, 2006 and references therein); (ii) recharge zones can be associated with lower temperature values compared to the discharge zones where the temperature is typically higher. The temperature may remain undisturbed in areas with lateral groundwater flow (Vugrinovich, 1989). The temperature anomalies documented in this study (Figs. 5 to 7), however, are unlikely to be affected by groundwater flow or by the cooling effects of soil moisture contents. Because the bedrock of the URF atop the Alborz anticline is not suitable to host an aquifer, and because in this arid region, the water table is very deep and lies beyond the reach of the seasonal temperature variations. The persistence of temperature anomalies over time (Fig. 5) is a further indication that the anomalies are not due to seasonal variation but instead arise as a result of subsurface processes.

The validation of the temperature anomalies using the *in-situ* measurements was found not to be straightforward and was prone to error. The systematic underestimation of temperature variability by the in-situ data is due to a variety of factors, but mostly due to differences in the timing of data collection (contributing to diurnal effects), the measurement depth (surface vs. subsurface), the measurement intervals (instantaneous measurements vs. measurements made over days), the scaling effects (point vs. pixel-wised measurements), and the sensory systems and sensing mechanism. However, the good correlation between these variables (Fig. 8) indicates that the residual (and absolute) temperature anomalies are authentically originating from a petroleum accumulation at depth. It is also an indication that the methodology used was successful in isolating and mapping the subsurface thermal anomalies.

An important aspect of the applied methodology is that by removing the effects of surface processes, it yields datasets that are comparable to shallow temperature measurements made at 1–3m depth. In other words, the combination of a land surface model with the remotely sensed surface temperature data can not only efficiently remove the diurnal effects from temperature data but may also overcome the intrinsically limited penetration depth of thermal remote sensing data that is generally within a few millimeters (Li et al., 2013). This promising methodology, however, appears to be most suitable for arid to semi-arid regions characterized by sparse vegetation cover and a deep-water table. In densely vegetated areas, the remotely sensed LST is mostly controlled by the transpiration of the plants rather than by the characteristics of the subsurface geological constituents (Li et al., 2013).

Previous studies have suggested that the surface temperature method may be able to predict the shape and the extent of the underlying petroleum reservoir. This possibility cannot confidently be tested here because of limited access to seismic and drilling data. Nonetheless, the anomalies derived from the numerical modeling approach appear to be apical in shape and to conform to the microseepage-affected areas on the one hand (See Fig. 14f in Asadzadeh and Souza Filho, 2020a) and to the boundary of the structural trap (Fig. 7) on the other. On this basis, the devised methodology may be helpful for targeting prospective reservoirs and may also provide an effective tool for interpreting fluid migration routes. Based on the results of this and previous studies, several prospective areas (corresponding to negative temperature anomalies in Fig. 7) could be suggested for follow-up exploration and drilling, complementing the results obtained from microseepage mapping studies.

5.1. The causes of temperature anomalies: a new insight

As noted above, the so-called Roberts model (Roberts, 1981) is put forward to explain the origin of positive thermal anomalies. Conversely, negative temperature patterns are attributed to the insulation effect of petroleum against the basement heat flow (Fons, 1999). The former interprets the anomalies as fossil heat in the basin (Merriam, 2004) whereas the latter is assumed to occur due to a contrast in the thermal conductivity between the petroleum-bearing reservoir and surrounding water-saturated rocks, which is estimated to be 2:1 or greater (Fons, 1999; McGee et al., 1989).

Factors that play a role in the development of surface temperature anomalies, however, are very diverse and also include lateral variations in the heat flux from the basement (Frone et al., 2015), the regional groundwater flow regime (Anderson, 2005; Ibrahim, 1994; Vugrinovich, 1989), deformation and structural complexity (Frone et al., 2015; McGee et al., 1989), hydrocarbon biodegradation near the surface (<10 m) (Commission, 1994), and the heat released by radiogenic sources (Contreras and Negrete-Aranda, 2014). Hence, any attempt to relate temperature anomalies exclusively to a single one of these factors would oversimplify the intricate process. This complexity may also be a reason behind the failure of current models in explaining the diversity of temperature anomalies (both positive and negative) over petroleum accumulations.

The structural deformation can result in either elevated or reduced temperature patterns at the crest of anticlines depending on the thermal conductivity of the deformed strata (Frone et al., 2015; Meyer and McGee, 1985). Where the deformed strata consist of shaley lithologies, the presence of radiogenic isotopes in these units can result in the generation of additional heat at the crest of the anticline. This heat source is reported to account for up to 20% of the observed heat flows over sedimentary basins (Contreras and Negrete-Aranda, 2014). Likewise, the biodegradation of hydrocarbons can cause positive temperature anomalies of up to 0.5°C at the surface and up to 2.0°C at ~2 m depth (e.g. Commission, 1994). The latter has been corroborated by observations at oil-contaminated aquifers wherein a temperature increase in the order of 2–6°C has been recorded at 2–4 m depth (corresponding to the methanotrophic zone) (Warren et al., 2011).

An important process that has been completely overlooked in this context is the possible relationships between temperature anomalies and microseepage systems. A microseepage system is typically characterized by the rapid, near-vertical migration of light hydrocarbons to the surface (Schumacher, 2000). Gas chimneys develop at a scale that can be observed in seismic data (Aminzadeh et al., 2001), and may therefore be responsible for large-scale heat transfer from subsurface reservoirs to the near-surface environment. The role of the cross-stratal chimney column in transferring heat has been investigated by Dentzer et al. (2018), and studies show that at least 79% of the onshore petroleum accumulations are associated with the manifestations of an active microseepage system at the surface or near-surface environment (Schumacher, 2000).

An important point to consider here is that fluid flow and heat transfer take place under coupled conditions. The partial differential equation to describe this phenomenon could have the following form (Xu et al., 2015):

$$\rho c \frac{\partial T}{\partial t} + \nabla(\rho_f c_f \nu_f T - k \nabla T) = q_H \quad (1)$$

where subscript f denotes the fluid phase, ν_f is the fluid velocity, T is temperature, k is thermal conductivity, ρc is the thermal capacity, t is time, and q_H is a heat source comprising, for example, a radiogenic heat source. The numerical solution of Eq. 1 analogous to what is presented in Frone et al. (2015) is out of the scope of this article, but this equation can help comprehend the variables that might play a role in shaping the surface temperature anomalies. Thus over a petroleum accumulation where an active microseepage system exists, the insulating effects of hydrocarbons against basement heat flow are partly or wholly counteracted by two major factors (i) the seepage of hydrocarbons as an agent of convective heat transfer ($\rho_f c_f \nu_f T$ term in Eq. 1) to the surface, (ii) the biodegradation of seeping hydrocarbons near the surface as a heat source (q_H term) escalating the temperature anomalies (Commission, 1994; Warren et al., 2011). Any changes in the mineralogy, physicochemistry, and physical properties of the chimney column (over a depth range of 60–600m) due to long-term hydrocarbon microseepage, however, can act in the opposite direction. Changing the physical properties of the rock strata may lead to a decrease in the thermal conductivity (k) of the sedimentary column (Abu-Hamdeh and Reeder, 2000), thus decreasing the rate of heat transfer to the surface. Observations show that across certain oil and gas fields, there is a tendency for the positive temperature anomalies to be damped near the surface (McGee et al., 1989), which supports the latter hypothesis.

The magnitude of a microseepage-related temperature anomaly can be determined from the volume and velocity of the migrating fluids. In the case of groundwater flow, movement velocities as small as 3.05×10^{-12} m/s have been reported to result in a temperature anomaly of ~1 °C in the sedimentary columns (Frone et al., 2015). Other studies report that flow rates ranging from 1 mm/day to 1cm/year may result in significant temperature changes in the overlying environment (Blackwell, 1986; Roberts, 1981). In the case of petroleum microseeps, although flux rates range from a few to tens of mg m^{-2} d^{-1} (possibly reaching hundreds of mg m^{-2} d^{-1} over widely tectonized terrains (Asadzadeh and Souza Filho, 2017)), the ascending fluid maintains very high velocities varying from less than 1 m/day to tens of meters per day (Schumacher, 2000). Therefore, the high velocity, low volume flow regime of a microseepage system could impact the shallow subsurface temperature pattern dynamically. Such effects would be maintained as long as the hydrocarbon fluid maintains its upward migration. In fact, the precise balance between the above-noted factors will contribute to shaping the temperature anomalies and will govern their type and characteristics. In extreme cases in which these factors exactly counteract each other, no meaningful anomalies would be recorded over petroliferous areas.

Thus far, it is not known what proportion of petroleum accumulations are associated with temperature anomalies of either positive or negative type. However, non-anomalous cases are reported to account for 10 to 25% of the overall statistics (Fons, 1999; Meyer and McGee, 1985). In other words, at least 75% of petroleum accumulations worldwide are expected to be associated with some form of temperature anomalies.

There are several lines of evidence that support our hypothesis and point toward the potential relationships between microseeps and temperature anomalies:

(i) the fact that temperature anomalies are confined to a depth between 1 to 5–7 km (Roberts, 1981),

(ii) (ii) the fact that the temperature anomalies conform to the outlines of an underlying petroleum reservoir (due to near-vertical migration of hydrocarbon microseeps) and that they appear as apical or halo-type anomalies over petroleum accumulations in a similar manner as to microseepage systems (as indicated in this study),

(iii) (iii) the dynamic nature of the phenomenon, and the fact that the most pronounced negative anomalies appear directly over the most productive petroleum reservoirs (Fons, 2000). This is probably due to a drop in the rate and velocity of the seeping hydrocarbons (as the agent of transferring heat to the surface) following the development of a field. This is also consistent with observations made over carbon sequestration sites (see below).

A thorough understanding of these processes demands advanced numerical modeling, which should be considered for future research. If proven correct, the proposed model could provide a new framework to understand the abnormal temperature patterns commonly observed not only above petroleum reservoirs but also within sedimentary basins around the world (e.g. (Frone et al., 2015)).

In the case of the Alborz oilfield, we speculate that the insulating effect of petroleum arising from the thick pay zone in combination with the blanketing effect of clay-rich strata near the surface and a low microseepage intensity in the area to counterbalance the heat flow could be parts of the reasons for the dominance of negative temperature anomalies. The low microseepage intensity is likely due to the presence of a very effective caprock comprised of thick evaporative units hindering the upward movement of hydrocarbons and heat. Two additional factors for a negative temperature anomaly in the area can be the absence of shale-rich lithologies at the crest of the Alborz anticline, which could have acted as a potential source of radiogenic heat, and historical production activities (including instances of a blowout in well 5-Alborz) within the field over the past decades. Understanding the interplay of these factors is crucial for unraveling the complex thermal dynamics of the region.

5.2. Implications for the monitoring of carbon sequestration sites

Similar to natural petroleum accumulations, carbon sequestration sites are prone to be associated with microseepage systems (Klusman, 2011; Verkerke et al., 2014), enabling the injected CO_2 to migrate upward toward the surface. If future studies further augment the relationships between petroleum microseepage and thermal anomalies, then the temperature anomalies would be expected to evolve/emerge over carbon sequestration sites accordingly; a phenomenon that has already been observed and demonstrated in several sequestration sites (Verkerke et al., 2014). Consequently, the temperature mapping technique based on satellite-derived LST data, as described and applied in this study, holds the potential to detect and monitor the areal extent of the induced CO_2 microseepage by visualizing the corresponding thermal anomalies.

6. Conclusion and outlook

This study has demonstrated that petroleum-related thermal anomalies are present in the remotely sensed nighttime temperature data from the Alborz oilfield, Central Iran and that the anomalies are consistent over time. An advanced numerical method provided by the SKinTES model was deployed successfully to highlight/segregate the contribution of subsurface heat flow from within the measured temperature data. It was shown that the modeling approach combined with satellite-derived temperature data can yield results that are comparable to shallow temperature measurements in terms of efficiency and effectiveness. A limitation of this technique, however, is that in its current form, it applies only to arid to semi-arid regions with sparse vegetation cover and exposed surfaces.

Although a negative temperature anomaly was detected in the Alborz area, either positive or negative temperature anomalies could be expected to emerge in the residual temperature anomaly map depending on the geological setting and the presence or absence of a petroleum microseepage system. For this reason, the yielded thermal anomalies must be carefully interpreted in the context of the lithology and structural geology of the area to get the best possible results out of this approach.

The advanced temperature mapping technique presented in this study could help broaden the application of remotely sensed temperature data not only in petroleum exploration but also in other geothermic fields, including geothermal exploration and monitoring. This becomes significant when knowing that high-resolution temperature data from the ASTER and the ECOSTRESS (ECOsystem Spaceborne Thermal Radiometer Experiment on board of the International Space Station) instruments are now available globally at no cost. Integrating this technique with other exploratory tools in general and remote sensing mapping techniques in particular (including surface alteration maps) could add synergy and help build a more effective methodology for surveying sedimentary basins for energy resources.

Acknowledgment

This work was financially supported by the Sao Paulo Research Foundation (FAPESP) under grant number 2017/25002-7. The authors are thankful to Francisco Ladeira, Masoud Mosavian, and Negar Kanani, respectively for providing field equipment, companionship during the fieldwork, and assistance in weather data acquisition. The Exploration Directorate of the National Iranian Oil Company (NIOC) is acknowledged for the logistics provided during the course of the field measurements. NASA's ASTER User Authorization Committee is thanked for granting us the privilege to acquire new thermal data. C.R.S. Filho acknowledges the support from the Brazilian National Council for Scientific and Technological Development (CNPq; grants #309712/2017-30 and 437337/2018-9).

Appendix A: Model description

SKinTES is a physically-based, single-source modeling approach designed to simulate LST over sparsely vegetated surfaces with NDVI <0.2, which can be applied to the measurements performed under clear-sky conditions (cloudiness <0.4). The model relies on remote sensing data for parameter estimation and can take into account the effects of complex topography and geology in the modeling processes. The only required ground data for model implementation are meteorological data (including air temperature, air pressure, wind speed, and relative humidity), which can typically be obtained from a nearby weather station (Asadzadeh and Souza Filho, 2023).

The temperature (T) profile in each pixel is obtained by a one-dimensional heat flow equation:

$$\frac{\partial T}{\partial t} = \kappa \frac{\partial^2 T}{\partial z^2} \quad \text{(A1)}$$

where t (s) and z (m) are time and depth, respectively, and κ $(m^2 s^{-1})$ is soil/rock thermal diffusivity. The lower boundary condition is considered to be a depth at which the temperature gradient is equal to zero (typically between 1–3 m). The upper boundary condition is determined by the energy balance equation at the interface of the Earth's surface and the atmosphere:

$$\mathrm{R_n} - \mathrm{H} - \lambda\mathrm{E} - \mathrm{G} = 0 \qquad \text{(A2)}$$

where R_n $(= S_g + R_a - R_g)$ is the surface net radiation, H (Wm^{-2}) is the sensible heat flux, λE is the latent heat flux, and G is the surface heat flux.

SKinTES employs the Penman-Monteith equation constrained by the evaporation coefficient to estimate the actual latent heat flux (λE), and the Monin-Obukhov similarity model to estimate the sensible heat flux (H). Over rugged terrain, the incoming shortwave radiation (S_g) is calculated as the sum of direct, diffuse, and terrain-reflected irradiances, which is achieved by integrating the direct and diffuse transmittance beams of the atmosphere from Yang's model with the surface albedo and the topographic parameters. The downwelling longwave radiation from the atmosphere (R_a) is obtained by applying Prata's model. The flow of water in porous soils/sediments is modeled using the linearized form of Richards's equation (Asadzadeh and Souza Filho, 2023).

The pixel-wise numerical solution of the energy balance, heat, and water flow equations provides an estimate of the dynamics of surface temperature changes over time. However, the temperature value at the end of the simulation interval is typically recorded. The results are then compiled into an image array and compared with the corresponding remote sensing data. For more detailed information regarding the theoretical basis of the SKinTES model and its parametrization scheme, the readers are referred to Asadzadeh and Souza Filho (2023).

Appendix B: Model setup

The broadband surface albedo (α_g) was computed from the topographically adjusted Level-2 Landsat-8 data (acquired on 9 August 2020) using an equation proposed by Liang (2001). The broadband surface emissivity (ε_g) was derived from the ASTER emissivity (AST05) product using the conversion coefficients proposed by Cheng et al. (2013). The thermal-optical trapezoid method was deployed to estimate the soil moisture content at the time of model initiation using ASTER data. The multispectral data in conjunction with the geologic map shown in Fig. 3 were used to map the surface roughness lengths. For this aim, the scene was segmented into eight land cover types including sandstone, salt, playa, alluvial deposits, fallow land, urban areas, roads, and vegetated areas. A z_{0m} value ranging between 0.0015 and 1.5m was assigned to each cover type. The clays and quartz contents of the area were estimated respectively from ASTER shortwave infrared and ASTER TIR data sets.

To map rock thermal properties, the area was partitioned into three broad segments -- sandstone, salt dome, and other constituents -- and representative values for thermal conductivity (3.0, 5.0, and 2.2 $\mathrm{Wm^{-1}K^{-1}}$), mean density (2800, 2200, and 2700 $\mathrm{kgm^{-3}}$), and solid heat capacity (2.8, 1.2, and 2.0 $\mathrm{MJm^{-3}K^{-1}}$) were assigned to each partition, respectively. The resulting maps were integrated by a modified form of the Johansen model (described in

Asadzadeh and Souza Filho, 2023) to derive the rock thermal properties, comprising the dry and the saturated thermal heat conductivities and the volumetric thermal heat capacity. Elevation data were derived from the ALOS dataset at 30m spatial resolution. The sky view factor was computed using a search radius of 20 pixels and 32 search directions. The slope and aspect were obtained by using the quadratic surface fitting method. All the raster datasets were stacked and resampled to 90 m spatial resolution to conform to the surface kinetic temperature data.

Initial conditions were set by feeding the analytic models defined in Asadzadeh and Souza Filho (2023) with pairs of day- and nighttime temperature data acquired on August 10 and 15, 2020, respectively. The same period was also used to spin up the model. The historic meteorological records were attained from the Qom weather station at 3-hour intervals and subsequently were interpolated into the time step of the model (i.e. 90 s) using the shape-preserving cubic spline method. A constant air temperature lapse rate of $-0.005°C.m^{-1}$ was used during the spatial gridding of air temperature data. In the model execution phase, the urban areas to the south of the oilfield were omitted to speed up the processing.

References

ABBASI, G., MOTAMEDI, H., ORANG, K. and NICKANDISH, A.A., 2020. Petroleum Geology of the Western Part of the Central Iran Basin. *Journal of Petroleum Geology*, **43,** 171-190.

ABU-HAMDEH, N.H. and REEDER, R.C., 2000. Soil thermal conductivity: Effects of density, moisture, salt concentration, and organic matter. *Soil Science Society of America Journal*, **64,** 1285–1290.

AMINZADEH, F., BERGE, T., B., DE GROOT, P. and VALENTI, G., 2001. Using Gas Chimneys as an Exploration Tool. *World Oil*, **222,** 50-56.

ANDERSON, M.P., 2005. Heat as a Ground Water Tracer. *Groundwater*, **43,** 951-968.

ASADZADEH, S. and SOUZA FILHO, C.R., 2017. Spectral remote sensing for onshore seepage characterization: A critical overview. *Earth-Science Reviews*, **168,** 48-72.

—, 2020a. Characterization of microseepage-induced diagenetic changes in the Upper-Red Formation, Qom region, Iran. Part I: Outcrop, geochemical, and remote sensing studies. *Marine and Petroleum Geology*, **113,** 104149.

—, 2020b. Characterization of microseepage-induced diagenetic changes in the Upper-Red Formation, Qom region, Iran. Part II: A new insight using reflectance spectroscopic analysis. *Marine and Petroleum Geology*, **117,** 104387.

—, 2023. Numerical Modeling of Land Surface Temperature over Complex Geologic Terrains: A Remote Sensing Approach. *Remote Sensing*, **15,** 4877.

BECKER, M.W., 2006. Potential for Satellite Remote Sensing of Ground Water. *Groundwater*, **44,** 306-318.

BLACKWELL, D.D., 1986. Use of heat flow/temperature measurements, including shallow measurements, in hydrocarbon exploration. In: DAVIDSON, M.J.s (Ed.): Unconventional methods in exploration for petroleum and natural gas. 321-350.

CHAKRABORTY, R., GUPTA, R.P. and AWASTHI, A.K., 2010. Model thermal anomalies over petroliferous basins. *Oil and Gas Journal*, **108,** 72-75.

CHENG, J., LIANG, S., YAO, Y. and ZHANG, X., 2013. Estimating the Optimal Broadband Emissivity Spectral Range for Calculating Surface Longwave Net Radiation. *IEEE Geoscience and Remote Sensing Letters*, **10,** 401-405.

COMMISSION, E., 1994. European Technologies for Oil and Gas Exploration in Remote and Poorly Accessible Areas. In., 26.

CONTRERAS, J. and NEGRETE-ARANDA, R., 2014. A 1.5D model of the steady-state thermal structure of detachment folds. *Marine and Petroleum Geology*, **54,** 96-105.

COOLBAUGH, M., KRATT, C., FALLACARO, A., CALVIN, W.M. and TARANIK, J.V., 2007. Detection of geothermal anomalies using Advanced Spaceborne Thermal Emission and Reflection Radiometer (ASTER) thermal infrared images at Bradys Hot Springs, Nevada, USA. *Remote Sensing of Environment*, **106,** 350-359.

DENTZER, J., BRUEL, D., DELESCLUSE, M., CHAMOT-ROOKE, N., BECCALETTO, L., LOPEZ, S., COURRIOUX, G. and VIOLETTE, S., 2018. Thermal and seismic hints for chimney type cross-stratal fluid flow in onshore basins. *Scientific Reports*, **8,** 15330.

EPPELBAUM, L., KUTASOV, I. and PILCHIN, A., 2014. Near-Surface Temperature Measurements. In: Applied Geothermics. 619-653.

FONS, L., 1984. Methods for Locating oil or Gas Deposits Employing Temperature and/or Geothermal Gradient Measurements. In: PATENT, U.S.s (Ed.).

—, 1999. Temperature method can help locate oil, gas deposits. *Oil and Gas Journal*, **97,** 58-64.

—, 2000. Temperature anomaly mapping identifeis subsurface hydrocarbons. *World Oil*, **221,** 65-69.

—, 2001. Finding, mapping temperature anomalies can aid oil, gas exploration. *Oil and Gas Journal*, **99,** 38-48.

FONS, L. and DONOVAN, J., 2000. Hydrocarbon Identification through Temperature Anomaly Mapping. *GCAGS*. Houston, Texas.

FRONE, Z.S., BLACKWELL, D.D., RICHARDS, M.C. and HORNBACH, M.J., 2015. Heat flow and thermal modeling of the Appalachian Basin, West Virginia. *Geosphere*, **11,** 1279-1290.

GUPTA, R.P., CHAKRABORTY, R. and AWASTHI, A.K., 2009. Satellite data can cost effectively show oil field thermal anomalies. *Oil and Gas Journal*, **107,** 34-36.

GUTIÉRREZ, F.J., LEMUS, M., PARADA, M.A., BENAVENTE, O.M. and AGUILERA, F.A., 2012. Contribution of ground surface altitude difference to thermal anomaly detection using satellite images: Application to volcanic/geothermal complexes in the Andes of Central Chile. *Journal of Volcanology and Geothermal Research*, **237-238,** 69-80.

IBRAHIM, M.W.I., 1994. Geothermal Gradient Anomalies of Hydrocarbon Entrapment, UKCS Quadrants 35 to 54. In: European Petroleum Computer Conference. 12.

KLUSMAN, R.W., 2011. Comparison of surface and near-surface geochemical methods for detection of gas microseepage from carbon dioxide sequestration. *International Journal of Greenhouse Gas Control*, **5,** 1369-1392.

LI, Z.-L., TANG, B.-H., WU, H., REN, H., YAN, G., WAN, Z., TRIGO, I.F. and SOBRINO, J.A., 2013. Satellite-derived land surface temperature: Current status and perspectives. *Remote Sensing of Environment*, **131,** 14-37.

LIANG, S., 2001. Narrowband to broadband conversions of land surface albedo I: Algorithms. *Remote Sensing of Environment*, **76,** 213-238.

MAJUMDAR, T.J., MITRA, D.S. and NASIPURI, P., 2010. Study of surface temperature anomalies over the oil fields in the Cambay Basin, India using Aster nighttime data. *International Journal of Geoinformatics*, **6,** 55-64.

MALBÉTEAU, Y., MERLIN, O., GASCOIN, S., GASTELLU, J.P., MATTAR, C., OLIVERA-GUERRA, L., KHABBA, S. and JARLAN, L., 2017. Normalizing land surface temperature data for elevation and illumination effects in mountainous areas: A case study using ASTER data over a steep-sided valley in Morocco. *Remote Sensing of Environment*, **189,** 25-39.

MCGEE, H.W., MEYER, H.J. and PRINGLE, T.R., 1989. Shallow geothermal anomalies overlying deeper oil and gas deposits in Rocky Mountain region. *AAPG Bulletin*, **73,** 576-597.

MERRIAM, D.E., 2004. Subsurface temperature as a passkey for exploration of mature basins: Hot anticlines–a key to discovery? *Oil and Gas Journal*, **102,** 29-35.

MEYER, H.J. and MCGEE, H.W., 1985. Oil and Gas Fields Accompanied by Geothermal Anomalies in Rocky Mountain Region. *AAPG Bulletin*, **69,** 933-945.

MORLEY, C.K., KONGWUNG, B., JULAPOUR, A.A., ABDOLGHAFOURIAN, M., HAJIAN, M., WAPLES, D., WARREN, J., OTTERDOOM, H., SRISURIYON, K. and KAZEMI, H., 2009. Structural development of a major late Cenozoic basin and transpressional belt in central Iran: The Central Basin in the Qom-Saveh area. *Geosphere*, **5,** 325-362.

MORLEY, C.K., WAPLES, D.W., BOONYASAKNANON, P., JULAPOUR, A. and LOVIRUCHSUTEE, P., 2013. The origin of separate oil and gas accumulations in adjacent anticlines in Central Iran. *Marine and Petroleum Geology* **44,** 96-111.

NASIPURI, P., MAJUMDAR, T.J. and MITRA, D.S., 2006. Study of high-resolution thermal inertia over western India oil fields using ASTER data. *Acta Astronautica*, **58,** 270-278.

PARFENENKO, N.V., 1979. Main Causes of Geothermal Anomalies Above Oil-Gas Fields. *Petroleum Geology: A digest of Russian literature on Petroleum Geology*, **16,** 507-509.

ROBERTS, W.H.I., 1981. Some uses of temperature data in petroleum exploration. In: GOTTLIEB, B.M.s (Ed.): Unconventional methods in exploration for petroleum and natural gas. 8-49.

ROMAGUERA, M., VAUGHAN, R.G., ETTEMA, J., IZQUIERDO-VERDIGUIER, E., HECKER, C.A. and VAN DER MEER, F.D., 2018. Detecting geothermal anomalies and evaluating LST geothermal component by combining thermal remote sensing time series and land surface model data. *Remote Sensing of Environment*, **204,** 534-552.

SCHUMACHER, D.D., 2000. Surface geochemical exploration for oil and gas: New life for an old technology. *The Leading Edge*, **19,** 258-261.

VERKERKE, J.L., WILLIAMS, D.J. and THOMA, E., 2014. Remote sensing of CO2 leakage from geologic sequestration projects. *International Journal of Applied Earth Observation and Geoinformation*, **31,** 67-77.

VUGRINOVICH, R., 1989. Subsurface temperatures and surface heat flow in the Michigan Basin and their relationships to regional subsurface fluid movement. *Marine and Petroleum Geology*, **6,** 60-70.

WARREN, E., BEKINS, B., SIHOTA, N. and CAMBELL-SWARZENGKI, P., 2011. Unsaturated zone temperature increase due to aerobic methanotropic activity. *GSA Annual Meeting*. Minneapolis, Minnesota.

XU, C., DOWD, P.A. and TIAN, Z.F., 2015. A simplified coupled hydro-thermal model for enhanced geothermal systems. *Applied Energy*, **140,** 135-145.

ZIELINSKI, G.W. and BRUCHHAUSEN, P.M., 1983. Shallow Temperatures and Thermal Regime in the Hydrocarbon Province of Tierra del Fuego1. *AAPG Bulletin*, **67,** 166-177.

Figure captions

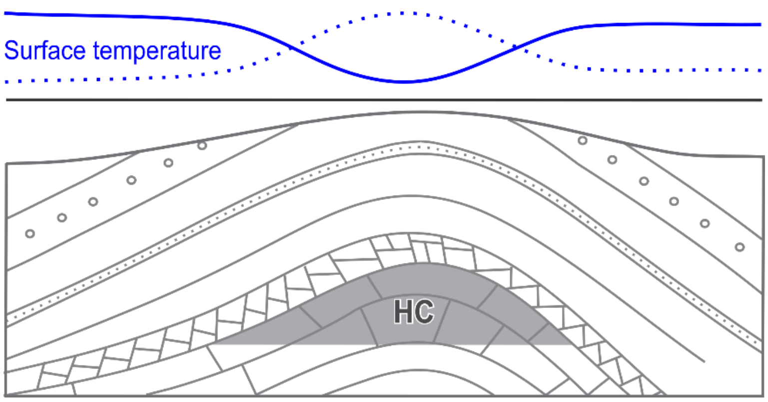

Fig. 1. Cartoon diagram showing the occurrence of positive and negative (near-) surface temperature patterns above petroleum accumulation in the subsurface.

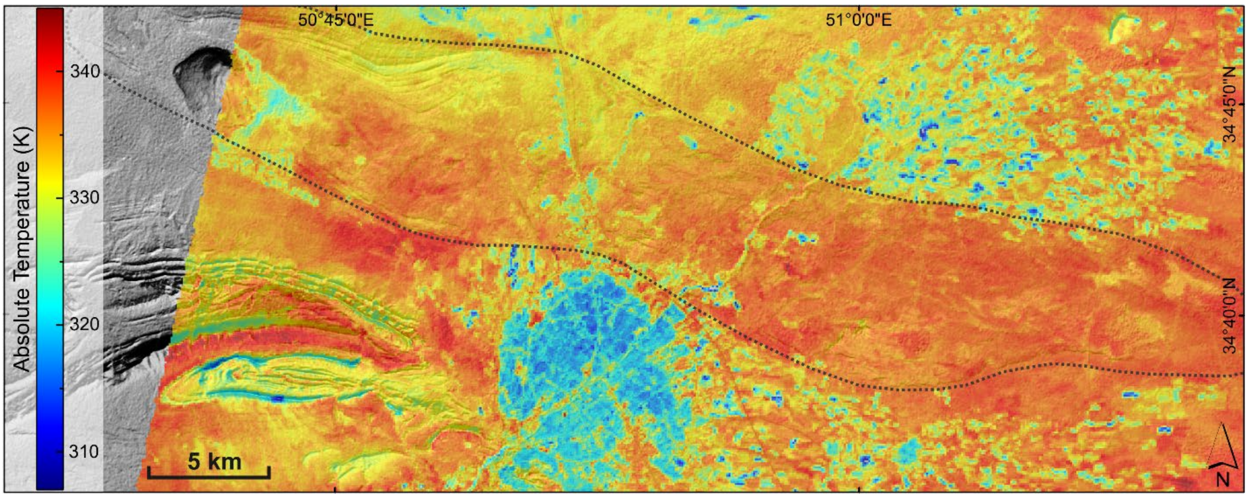

Fig. 2. Daytime ASTER kinetic temperature image over the Alborz oilfield (outlined by the black dotted line) near Qom city (blue area in the bottom center), Central Iran, acquired on 10 August 2020 at 10:30 a.m. local time. The surface temperature data appear to be overwhelmed by the warming effect of insolation.

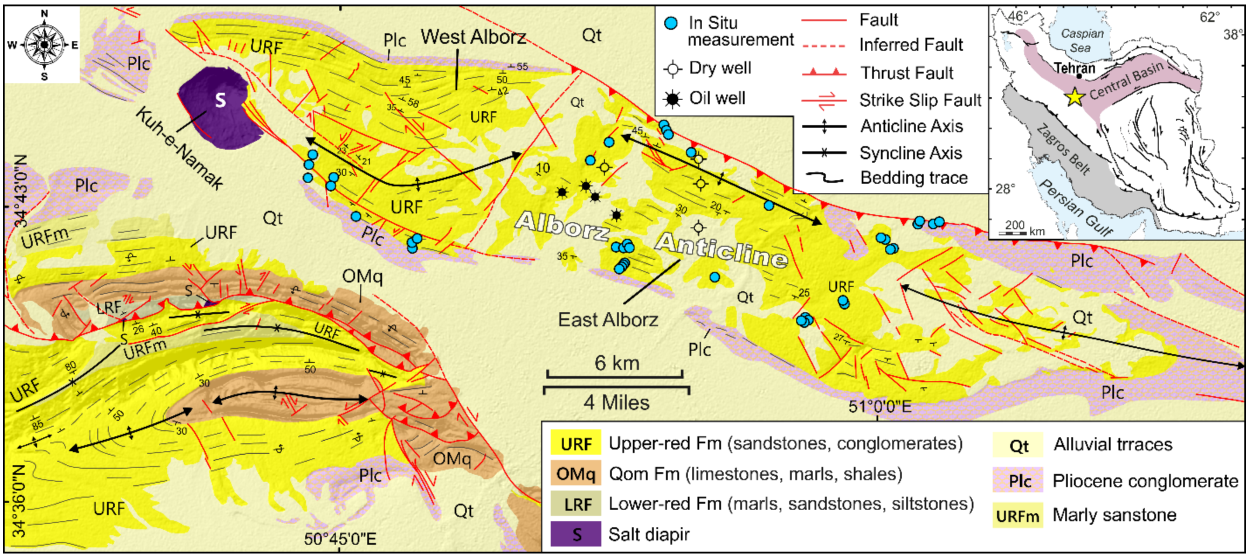

Fig. 3. Generalized geologic map of the study area in the Qom region, Iran (modified after Asadzadeh and Souza Filho, 2020a). The blue circles represent the sites of *in-situ* temperature measurements. Fm = Formation. The inset map displays the locality of the area (yellow star) in Iran.

Fig 4. Field photograph of *in situ* temperature measurements being made (a) at the surface and (b) in an auger-drilled hole of ∼15–20 cm deep.

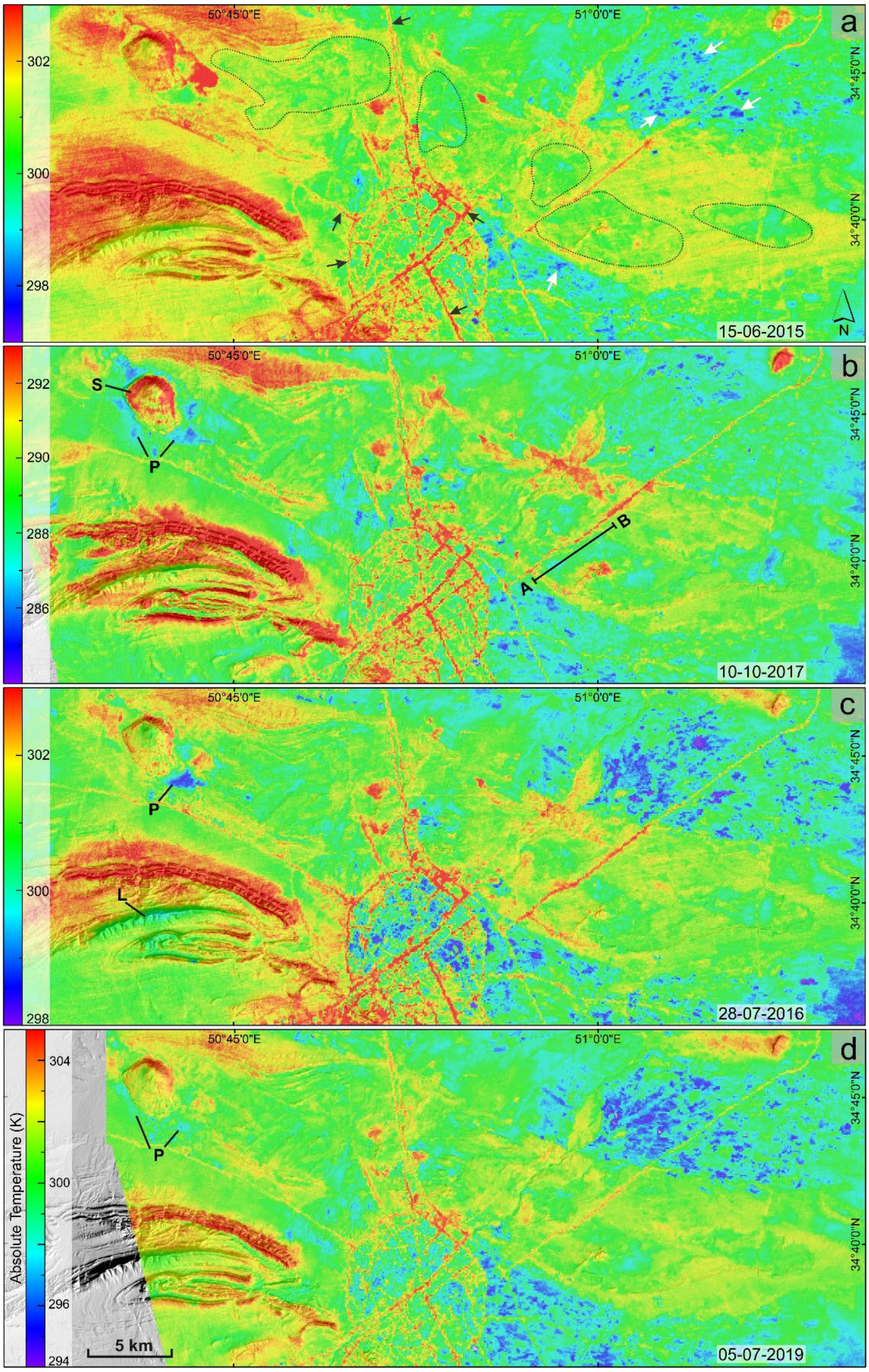

Fig. 5. Land surface temperature maps of the study area derived from ASTER nighttime data collected on four different dates: (a) 15 June 2015, (b) 10 October 2017, (c) 28 July 2016, and (d) 5 July 2019. All maps are superimposed on a shaded-relief digital elevation model. The black dotted polygons in (a) outline the low-temperature anomalies detected over petroleum-bearing zones, and the black and white arrows point toward paved roads and vegetated areas, respectively. A–B in (b) corresponds to

the temperature profile (solid line) in Fig. 6. S = salt diapir, P = playa, L = elevated topography affected by the air temperature's lapse rate.

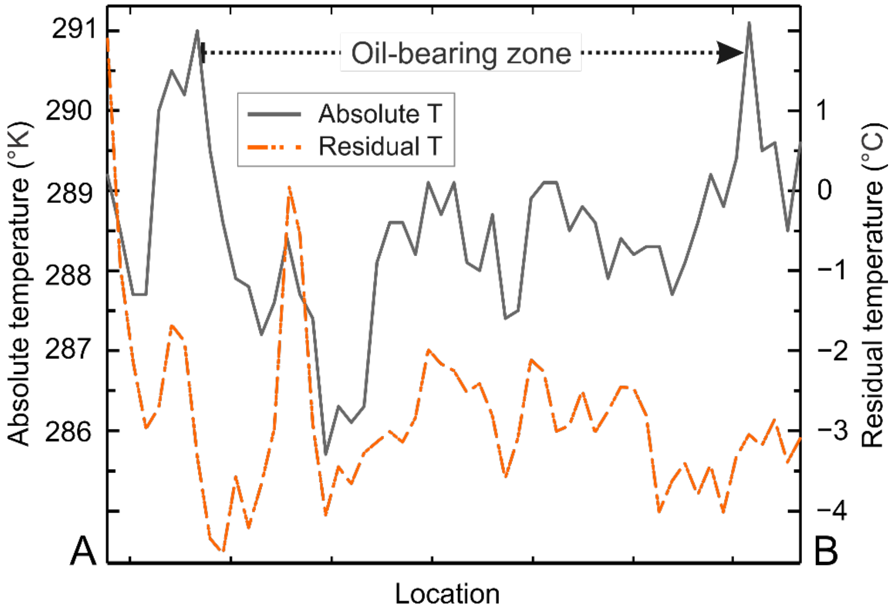

Fig. 6. Absolute and residual temperature profiles over the oil-bearing extent of the Alborz oilfield corresponding to the profile line A–B in Figs. 5b and 7. Both temperature profiles are representative of low/negative temperature anomalies.

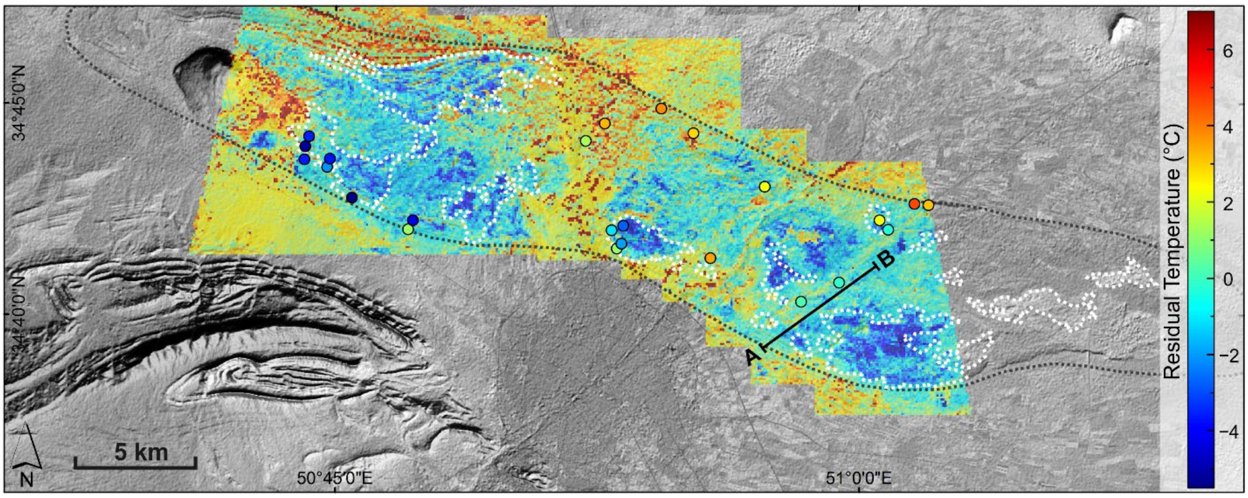

Fig. 7. Residual temperature anomaly map obtained by subtracting the model-simulated image data from the ASTER-derived kinetic temperature product. The dotted black line indicates the boundary of the Alborz anticline and the dotted white lines represent the outline of the microseepage-affected areas as mapped by Asadzadeh and Souza Filho (2020a). A–B corresponds to the temperature profile depicted in Fig. 6. The color circles represent *in-situ* temperature data measured in shallow holes. Note that the modeled area is constrained by the overlap of day-, and nighttime thermal data to the left and right, respectively. The northern and southern limits were excluded to speed up the processing.

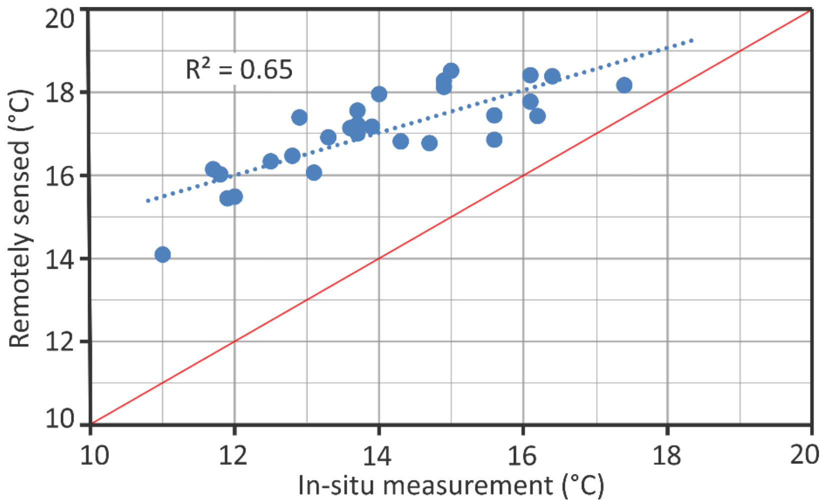

Fig. 8. Scatter-plot showing the close relationships between *in-situ* temperature measurements made at shallow (~15–20 cm) drill holes and the corresponding pixel values derived from the remotely sensed kinetic surface temperature data collected on 10 October 2017 by the ASTER instrument. The 1-to-1 line is depicted in solid red.